ERAstar: a High Resolution Ocean Forcing Product

Ana Trindade, Marcos Portabella, Ad Stoffelen, Wenming Lin, and Anton Verhoef

***Abstract*—To address the growing demand for accurate high-resolution ocean wind forcing from the ocean modeling community, we develop a new forcing product, ERA*, by means of a geolocated scatterometer-based correction applied to the ECMWF ERA-interim reanalysis (ERAi). This method successfully corrects for local wind vector biases present in the ERAi output globally. Several configurations of the ERA* are tested using complementary scatterometer data (ASCAT-A/B and OSCAT) accumulated over different temporal windows, verified against independent scatterometer data (HSCAT) and evaluated through spectral analysis to assess the geophysical consistency of the new stress equivalent wind fields (U10S). Due to the high quality of the scatterometer U10S, ERA* contains some of the physical processes missing or misrepresented in ERAi. Although the method is highly dependent on sampling, it shows potential, notably in the tropics. Short temporal windows are preferred, to avoid oversmoothing of the U10S fields. Thus, corrections based on increased scatterometer sampling (use of multiple scatterometers) are required to capture the detailed forcing errors. When verified against HSCAT, the ERA* configurations based on multiple scatterometers reduce the vector root mean square difference about 10% with respect to that of ERAi. ERA* also shows a significant increase in small-scale true wind variability, observed in the U10S spectral slopes. In particular, the ERA* spectral slopes consistently lay between those of HSCAT and ERAi, but closer to HSCAT, suggesting that ERA* effectively adds spatial scales of about 50 km, substantially smaller than those resolved by global NWP output over the open ocean (about 150 km).**

***Index Terms*—ERA*, Scatterometer Wind, NWP, Ocean Wind Forcing, Oceanic Mesoscale, Scatterometer Correction.**

I. Introduction

HIGH-resolution ocean modelling studies are essential to understand the processes that occur in the ocean and at the sea surface. In a simplified manner, physical ocean models, whether global or regional circulation models, are used for numerical simulations, either integrated as modules of earth system models (usually for climate simulations) or used as coupled or stand-alone models. While for stand-alone models, the initial and the forcing boundary conditions, i.e., momentum and heat fluxes, are usually obtained from a data set, for coupled models, e.g., coupled ocean-atmosphere models, boundary layer fluxes are computed by an atmospheric model and fed into the ocean model, while surface information from the latter may be fed into the former, i.e., there is a feedback mechanism at play, part of the earth system dynamics [1].

Because much of the ocean's variability, especially in the top layers, is wind driven, it is crucial to choose an accurate wind forcing product, which is able to resolve the fine ocean scales. Scatterometers provide high resolution surface wind measurements, but only twice a day. In the absence of high spatial and temporal resolution global sea surface wind data observations, Numerical Weather Prediction (NWP) forcing products are widely used in ocean forecasting. Among the most commonly simulated atmospheric wind fields are those generated by the Integrated Forecast System (IFS) or Global Circulation Models (GCM), e.g., the European Centre for Medium-range Weather Forecasts (ECMWF) reanalysis or ERA-interim (hereafter referred to as ERAi), or locally downscaled versions of it (http://projects.knmi.nl/knw/).

Although ubiquitous, prior to being used as ocean forcing (i.e., wind stress), the NWP output requires additional information on ocean currents, atmospheric stratification and mass density. Moreover, although frequently used for ocean simulations, several issues with global NWP output (like ERAi) have been reported, e.g., large-scale circulation errors ([2]), misplacement of fronts and depressions, poorly resolved small-scale dynamics, such as those associated with moist convection ([3]), or lack of crossisobaric flow (i.e., NWP wind directions are biased with respect to the observed winds with opposite sign in the Southern and the Northern Hemispheres, particularly in stable stratification) [4], [5], [6].

In contrast, ocean surface vector winds derived from scatterometers onboard Earth Observation (EO) satellites, although intrinsically limited by temporal and spatial sampling, exhibit considerable spatial detail and accuracy on the sea surface winds [7], [8]. In addition, while NWP wind outputs are relative to a fixed Earth grid, scatterometers measure the wind relative to the moving ocean surface, i.e., provide the ocean forcing [9]. Hence, in contrast with NWP, air-sea fluxes of momentum and heat can be accurately determined from scatterometer data [10], [11], and in highly energetic oceanic regions like the western boundary current systems, the ocean currents and mesoscale eddies are accounted for.

Furthermore, [12], [7], [13] established that while the effective resolution of scatterometer winds is about 25 km, that of the global NWP winds is about 100-200 km (i.e., the latter are unable to properly resolve small-scale wind variability).

The NWP output therefore misses relevant ocean-atmosphere interaction at both large scales and at the oceanic mesoscale. In line with the latter, [14] filter and find persistent mesoscale features in scatterometer winds (i.e., 4-year averages of 25 km QuikSCAT winds) that are missing in the model wind fields. In addition, [2] describe the large-scale circulation NWP errors in ERA. These persistent features give rise to systematic differences between scatterometer and NWP sea surface winds that have been monitored since the launch of the European Remote Sensing Satellite (ERS-1) in 1991 [4]. Such systematic differences are hereafter referred to as local biases that persist over time, and are visible when scatterometer and model winds are collocated. They mostly represent unresolved geophysical processes by NWP models.

In this regard, note that mesoscale variability due to atmospheric dynamics has time scales of only a few hours,

while ocean mesoscale dynamics varies over days. Hence, the large-scale atmospheric circulation errors and induced oceanic mesoscale variability errors in the surface winds, may be corrected by averaging over a few days, while variable errors in mesoscale atmospheric dynamics or due to moist convection cannot be corrected this way.

In light of this, attempts to combine scatterometer measurements and NWP estimates (in blended products and data assimilation) allow for increased temporal resolution products, but are affected by the spatial characteristics and caveats of the NWP models, as noted above. In particular, blending products representing different spatial scales, different geophysical processes and with systematic biases in geophysical variables and/or large-scale circulation errors, will result in a blended product with rather artificial and mixed spatiotemporal characteristics, depending on where the satellite measures, where the gaps are and how the local transient weather evolves. The currently most advanced method of blending consists in NWP data assimilation, though also here fundamental issues arise. A main problem is that NWP data assimilation uses the so-called BLUE paradigm, denoting Best Linear Unbiased Estimation, where the existence of biases as noted above obviously conflicts with this paradigm [15]. We further note that the biases in case of scatterometer winds are substantial [2] and where the bias correction method elaborated here, may be rather useful for NWP data assimilation in the future through better following the BLUE paradigm. Nevertheless, today scatterometer winds do improve the dynamical initialization of the weather phenomena, at least of those, which are well captured after the dynamical closure of NWP models. We further note that NWP data assimilation acts as a low pass filter, where small observed scales are ignored and mainly low atmospheric wave numbers are analyzed [16]. Finally, NWP model biases in large-scale circulation and parameterizations are restored within a few time steps of model integration after the initialization (analysis step). Therefore, the short-range forecast corrections as derived in this manuscript do not much depend on whether scatterometer winds are assimilated or not; see also [2].

In this study, a new ocean wind forcing product, ERA*, is developed. ERA* consists of a scatterometer-based correction (SC) of the mentioned systematic and persistent effects present in the ERAi output. The rationale of this method is that when the scatterometer wind data are accumulated over short periods of time, it is possible to overcome sampling errors and maintain some of the scatterometers most beneficial features, i.e., those related to relatively small-scale ocean processes, such as wind-current interaction, and furthermore, correct the large-scale NWP parameterization and dynamical errors. At the same time, the variability over the accumulation time due to fast processes, such as the variability due to moist convection and other transient errors is removed. This is, the ERA* would compute the accurately observed local mean differences to wind scatterometers over a few days. A running mean would reassure the time and space coverage of the original ERA atmospheric model fields.

With this approach, a scatterometer-based correction, using accurate, unbiased, high spatial resolution ocean vector winds from several scatterometers, i.e., the Advanced Scatterometers (ASCATs) on board Metop satellites [17] and the OSCAT scatterometer that flew on Oceansat-2, is developed.

The proposed correction consists of geo-located temporally averaged wind component differences between the scatterometer wind sources and the collocated NWP winds. The latter correspond to the aforementioned global reanalysis of ERAi 10-m neutral winds [18] produced by ECMWF, which are then corrected for atmospheric stability and air mass density effects, leading to the so-called 10-m stress-equivalent winds (U10S). The reason for converting ERAi wind output into U10S is to make ERAi output more compatible with scatterometer retrievals, which have been recently re-defined as U10S ([19]) as follows:

$$U10S = U10N\sqrt{\frac{\rho_{air}}{<\rho_{air}>}} \quad (1)$$

where U10N is the 10-m equivalent neutral winds, ρ_{air} the local air density and $<\rho_{air}>$ is the average global air density taken as 1.225 $[kg/m^3]$ (detailed description in [19]).

To efficiently reduce NWP local biases, a trade-off between optimal scatterometer sampling and the ability to keep the small spatial and temporal ocean induced scales is required. The scatterometer sampling characteristics have a large impact on the effectiveness of this method.

A relevant limitation is that scatterometer spatial sampling is non-uniform, i.e., it varies with both the latitude and the longitude, resulting in reduced coverage over the tropics when compared to other latitudes. Still, in-time accumulation of data from the different scatterometers allows for a significant reduction in revisit time [20]. Additionally, ERAi local biases are relatively persistent over time but such persistence is also regionally dependent, e.g., is longer in the trades than in rest of the tropics and higher latitudes. As such, different configurations of ERA*, with different temporal windows (from 1 to 5 days) and varying number of scatterometers (different combinations of the above-mentioned scatterometer systems) are tested to find the best quality general ocean forcing product. Furthermore, we explore the benefits of a configuration with multiple scatterometers and address the effects of sampling on the Level 4 (L4) wind product.

Regarding the temporal sampling effects, an interesting aspect of the scatterometer constellation is that each scatterometer passes at different times of day. The associated polar satellites are sun-synchronous and have a Local Time of Ascending Node (LTAN) that is fixed, i.e., the scatterometer and ERAi wind differences are always taken at about the same time of day. The ERAi diurnal cycle may be somewhat underestimated [20], [21], which could affect the applicability of ERA* at other times of day. Fortunately, we are able to verify ERA* by comparison to the independent HY-2A scatterometer winds at 6:00/18:00 LTAN.

This paper addresses the need for high-resolution ocean forcing by means of a L4 wind product that includes scatterometer-based corrections to ERAi, available every 3 hours. Section II introduces the data sets used in this study. Section III provides a detailed description of the ERA* methodology. In Section IV, a comprehensive verification of the ERA* product, using independent scatterometer data

(HSCAT on-board HY-2A) and spectral analysis, is carried out. Finally, the concluding remarks can be found in Section V.

II. Data sets

Four U10S products derived from different scatterometer systems, i.e., the Advanced Scatterometers (ASCAT) A and B onboard Metop-A and B, the Oceansat-2 scatterometer (OSCAT), and the HY-2A scatterometer (HSCAT), are used in this study for the year 2013. These scatterometers fly in different sun-synchronous orbits: the equator crossing Local Time of the Ascending Node (LTAN) is at 21:30 UTC, OSCAT is at 12:00 UTC, and HSCAT is at 18:00 UTC, while the descending node is 12 hours later/earlier. ASCAT-A & B operate at C-band and are therefore hardly affected by the presence of rain ([22], [23], [8]). OSCAT and HSCAT operate at Ku-band and are sensitive to both rain ([24], [25], [26]) and SST ([27], [28]). As such, using the inversion residual based on the methodologies in [24], [29] only about 0.5-1% of the ASCAT-A/B retrieved winds are quality controlled (QCed), while 5-7% of OSCAT/HSCAT winds are filtered out. As shown in [30], the OSCAT QC is mainly activated in the rainy areas of the east-west oriented bands in the tropics, particularly in the Western Pacific, thus considerably reducing the wind sampling in those areas. Note though that Ku-band rotating pencil-beam scatterometers (like OSCAT and HSCAT) have a wider swath (around 1500-1700 km) than ASCAT (1100 km). In spite of that,, due to their different spatial and temporal sampling characteristics, combining data from the C-band and Ku-band scatterometers results in a rather consistent data set for developing an ocean forcing product.

The HSCAT Level-1B (L1B) data set was provided by the National Ocean Satellite Application Center (NSOAS) and reprocessed with the Eumetsat Numerical Weather Prediction Satellite Application Facility (NWP SAF) Pencil-beam Wind Processor (PenWP) to Level 2 (L2) winds at 25-km swath grid spacing. Both ASCAT-A/B and OSCAT 12.5-km and 25-km, respectively, L2 products were provided by the Eumetsat Ocean and Sea Ice (OSI) SAF. The optimal viewing geometry and high radiometric resolution of the ASCAT-A/B fixed fan beams results in higher accuracy and resolution winds than those from rotating pencil-beam systems like OSCAT and HSCAT (e.g., [31], [32], [7]). However, note that the latter have been thoroughly validated and found to be of good quality (e.g., [33], [34], [35]) and largely consistent with ASCAT.

ASCAT and OSCAT L2 wind data are spatially interpolated from swath to a regular 12.5 x 12.5 km grid Level 3 (L3) using the Royal Netherlands Meteorological Institute (KNMI) genscat tool packages, distributed with the wind processors.

Verification with HSCAT in Section IV-B is done on the same L3 grid. For such purposes, the ERAi and the ERA* fields are collocated to the HSCAT swath using the PenWP and spatially interpolated to the regular grid, using the same tools as for ASCAT-A/B and OSCAT.

The ERAi data set is retrieved from the ECMWF's Meteorological Archival and Retrieval System (MARS) in a reduced Gaussian grid (N128) for the same period (2013). ERAi winds are then converted to U10S for consistency with the current scatterometer definition, using a stand-alone version of the ECMWF surface layer model [36]. Like the previous data sets, the ERAi U10S are also interpolated to the L3 grid with a field interpolation software (INTF) provided by ECMWF.

III. Methodology

The proposed methodology generates a scatterometer-based correction (SC) to produce ERA*, which is applied to both the zonal and the meridional wind components (u_{10s}, v_{10s}). Note that since the same formulation is used to correct the biases in both wind components, for simplicity, only the zonal component equations are shown in this Section.

The correction is based on the temporally averaged difference between scatterometer (u_{10s}^{SCAT}) and ERAi U10S (u_{10s}^{ERAi}), at grid point (*i,j*) and time sample (*t*), as described in Eq. 2.

$$SC(i,j,t_f) = \frac{1}{M}\sum_{t=1}^{M}(u_{10s}^{SCAT_k}(i,j,t) - u_{10s}^{ERAi}(i,j,t)) \quad (2)$$

Here, $u_{10s}^{SCAT_k}$ and u_{10s}^{ERAi}, respectively, correspond to the collocated scatterometer and ERAi zonal U10S component, in which k refers to the number of sensors used in the SC. The data sets are collocated for a temporal window of N days, centered at t_f, i.e., $t_f \pm N/2$ days, where M is the number of scatterometer and ERA collocations at grid point (i,j) within the defined time window around the ERAi time t_f.

Finally, the scatterometer correction, $SC(i,j,t_f)$ is added to the ERAi U10S forecasts, $u_{10s}^{ERA}(i,j,t_f)$ at time t_f (Eq. 3).

$$u_{10s}^{ERA*}(i,j,t_f) = u_{10s}^{ERAi}(i,j,t_f) + SC(i,j,t_f) \quad (3)$$

The ocean forcing product derived from Eq. 3, u_{10s}^{ERA*}, has a grid resolution of 12.5 km x 12.5 km and temporal resolution of 3 h, following ERAi.

Since scatterometer measurements from different sensors are combined, the effects of the instrument sampling errors on the quality of the generated wind data set can be addressed.

Thus, if $k = 1, 2, 3, 4$ then $u_{10s}^{SCAT_k}$ includes measurements going from a single scatterometer to multiple sensor combinations (see Table I for a summary of the different ERA* configurations).

Specifically, $k = 1$ contains ASCAT-A data, $k = 2$, combines both C-band radars (ASCAT-A and ASCAT-B), $k = 3$ combines ASCAT-A and OSCAT, and $k = 4$ uses all three sensors. Note that the last two k's combine observations from scatterometers working at different frequencies, i.e., ASCAT-A/B and OSCAT, respectively at 5.2 GHz (C-band) and 13.5 GHz (Ku-band).

Note that due to poor scatterometer sampling, some SC configurations will have gaps. By construction, these gaps are filled with ERAi winds only, i.e., ERA* winds will be the same as ERAi winds (see Eq. 2). In particular, for a 1-day and ASCAT-A based correction in the tropics, there is about 37.9% of gaps. In contrast, for a 2-day (or longer) time window and two complementary scatterometers (e.g., ASCAT-A and OSCAT), there is less than 0.3% of gaps.

Additionally, because we conduct our study with 2013 data, we use the available reprocessed scatterometer data sets and assume good inter-calibration between sensors, although these data sets do not account for latitude-depend biases due to SST and associated with wind speed PDF differences [27], [28]. Furthermore, the effects of Ku-band SST errors, is only about 0.02 m/s per Kelvin and relevant on a global scale, where SST varies by 30 K. The remaining local wind observation errors are typically more than a factor of two smaller than NWP model errors

Note that [37] and [38] explore an alternative bias mitigation approach to improve storm surge forecasting. While their method is applied regionally (in the Golf of Lyon) with the aim to correct wind speed biases by scaling the model winds with weighted scatterometer corrections averaged over a fixed time window (three days), the methodology presented is applied to the wind vector biases globally using multiple scatterometers and exploring several temporal windows.

IV. ERA* PRODUCT CHARACTERIZATION

In this section, a comprehensive characterization of the new ERA* U10S product is presented. First, a qualitative comparison between the ERA and ERA* products is shown in section IV-A. Then, the U10S quality is assessed against independent scatterometer observations (i.e., HSCAT) in section IV-B, and the geophysical consistency of the derived maps is assessed through spectral analysis in section IV-C. HSCAT observations, unlike buoys, are accurate relative to ocean surface currents that resolve the same oceanic variability scales that ERA* intends to capture.

A. Systematic local differences

Local systematic differences between collocated scatterometer and ERAi are generally within $\pm$ 2 $m.s^{-1}$, see Fig. 1. These differences are most noticeable where physical processes are misrepresented or absent in the model, therefore very pronounced over the western boundary ocean current systems (WBCS, i.e., the Agulhas current, the Gulf Stream or the Kuroshio current), the Antarctic Circumpolar Current (ACC), and in adjacent regions where the eddies generated by these currents detach. Likewise, in the tropics (see, e.g., the Inter Tropical Convergence Zone or ITCZ), U10S differences (particularly in the meridional component in Fig. 1(b)) are notable where the model winds are unable to capture both the detailed and large-scale wind circulation.

Local wind effects like see breeze, katabatic flows, corner winds or wind funneling effects (gap winds) are also visible in Fig. 1. The latter are readily evident from the meridional component in Fig. 1(b), e.g., see the gap wind effect in the Gulf of Tehuantepec (Central America, south of Mexico). Apart from the increase in wind speed, gap winds also strengthen tidal currents, furthermore affecting ocean circulation.

Although these differences are observed globally, the high latitudes, i.e., above 55°N and below 55°S, are excluded from this first version of the product. In fact, at high latitudes, the abundant (sun-synchronous) satellite sampling is expected to be optimal to model local bias reduction. However, a dedicated study is required to appropriately account for SST and the seasonality of the sea ice extent and its impact on the scatterometer wind-retrieval errors, quality control, and sampling. Moreover, the dynamical weather errors are more transient at high latitudes, probably resulting in a different optimum averaging period (see below).

Fig. 2 shows an ERAi U10S global map and its corresponding ERA* generated with a three-scatterometer based correction (i.e., ASCAT-A, ASCAT-B, and OSCAT) over a one-day temporal window (ERA*$_{ABO}$N1). By simply comparing ERAi and ERA*$_{ABO}$N1 U10S global maps, it is clear that the latter contains additional small scale variance when compared with the former (Fig. 2(a) is smoother than Fig. 2(b)), notably at the same locations where larger local biases emerge in Fig. 1(b).

In this line, Fig. 2(a) differs from Fig. 2(b) in that the increased variability seen in the latter should better capture the stationary signal from WBCS, the wind shadowing effects in the vicinity of islands, and the coastal effects associated to coastal orography.

An example of the aforementioned wind variability in the tropics, is given in Fig. 3 (see Table I for the naming convention of all ERA* configurations used). The Figure shows a zoom over the tropical Atlantic for the two products in Fig. 2 (see red box), and for another ERA* product generated with a larger temporal window of three days (ERA*$_{ABO}$N3). Fig. 3(b), arguably shows moist convection induced variability south of the West African coast, clearly visible in the ERA*$_{ABO}$N1, but not in the ERAi (Fig. 3(a)). Although somewhat smoothed, enhanced variability is also observed in the ERA*$_{ABO}$N3 map (Fig. 3(c)). The use of a longer temporal window in ERA*$_{ABO}$N3 than in ERA*$_{ABO}$N1 is responsible for the additional smoothing of the wind fields of the former, but also for the reduction of scatterometer weather sampling errors. This probably indicates that the ERA*$_{ABO}$N1 captures small-scale variability associated with relatively fast evolving atmospheric phenomena, while the ERA*$_{ABO}$N3 does not. Note also that this increased variability is attributed to moist convection, because it can be depicted by the scatterometers (due to updrafts and downdraft), in agreement with the findings of [39], [8], [3] over the tropical band. Although moist convection impacts the ocean exchange processes of momentum, heat and moisture and is fundamental to ocean model forcing, it cannot be fully resolved using a static mean correction, since the SC likely misses the highly variable component in moist convection (wind changes up to 15 m/s over a 30 min window). Due to the fast weather evolution during a satellite orbit, ERA*$_{ABO}$N1 clearly shows some small-amplitude jumps or artifacts (see, e.g., several straight lines in the top-left quadrant of Fig. 3(b)), which are not visible in the ERA*$_{ABO}$N3 (Fig. 3(c)), which smooths weather effects over 3 days. Such artifacts are associated with the edges of the different scatterometer swaths used, indicating that the 1-day corrections (N1) are based on relatively poor scatterometer weather sampling at these latitudes. Moreover, although such jumps may be small, they certainly become more evident in wind derivative products, such as divergence or curl (not shown).

TABLE I
ERA* GENERATED PRODUCTS ACCORDING TO THE NUMBER OF SENSORS AND TEMPORAL WINDOW USED TO CORRECT THE ERAI FORECASTS.

Data Source \ Temporal Window	1-d	2-d	3-d	4-d	5-d
ASCAT-A	ERA*$_A$N1	ERA*$_A$N2	ERA*$_A$N3	ERA*$_A$N4	ERA*$_A$N5
ASCAT-A, ASCAT-B	ERA*$_{AB}$N1	ERA*$_{AB}$N2	ERA*$_{AB}$N3	ERA*$_{AB}$N4	ERA*$_{AB}$N5
ASCAT-A,OSCAT	ERA*$_{AO}$N1	ERA*$_{AO}$N2	ERA*$_{AO}$N3	ERA*$_{AO}$N4	ERA*$_{AO}$N5
ASCAT-A,ASCAT-B,OSCAT	ERA*$_{ABO}$N1	ERA*$_{ABO}$N2	ERA*$_{ABO}$N3	ERA*$_{ABO}$N4	ERA*$_{ABO}$N5

Additional variance as seen in these global and regional maps of the ERA* meridional wind component manifests alike in all the ERA* configurations in Table I and in the zonal component of the wind (not shown), indicative of persistent mesoscale (ocean) variability. A more quantitative validation is presented in the next sections in order to verify and complete the preliminary conclusions drawn from the qualitative comparison presented in this section.

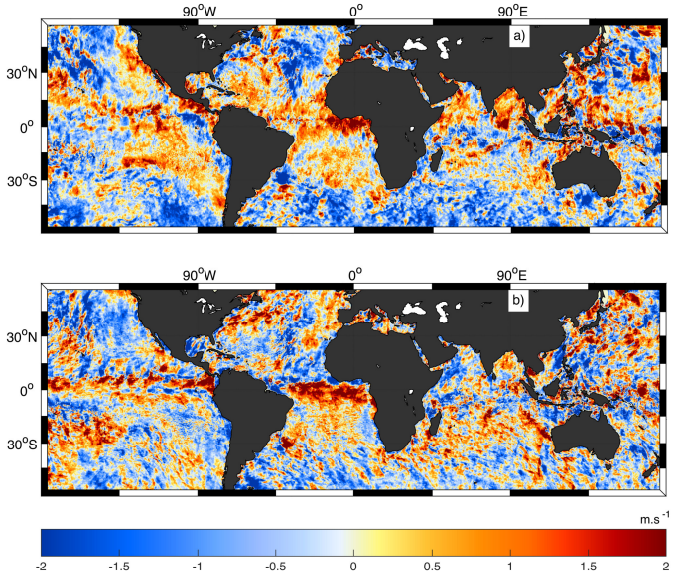

Fig. 1. Scatterometer Correction (SC) for a given day, i.e., 15^{th} January 2013. Collocated differences between ASCAT-A (12.5 km) and ERAi U10S for the zonal 1(a) and the meridional 1(b) wind components, accumulated over a 5-day temporal window centered around 06 UTC. The colors represent the differences in $m.s^{-1}$ (see color scale).

B. U10S verification

In section IV-A a qualitative assessment of ERA* wind maps reveals enhanced variability with respect to the original ERA wind. In this section we check whether this additional variance is dominated by true wind signal rather than noise, by assessing the quality of the different ERA* gridded ocean forcing products (i.e., using different SCs and temporal window combinations as shown in Table I) against independent U10S data.

The ERA* products are validated against independent scatterometer data, i.e., the 25 km HSCAT U10S product. HSCAT is a good wind reference since the orbit pass (6 am/6 pm) is very different from that of the instruments used to correct the ERA fields, i.e., ASCAT-A/B at 9:30 am/9:30 pm and

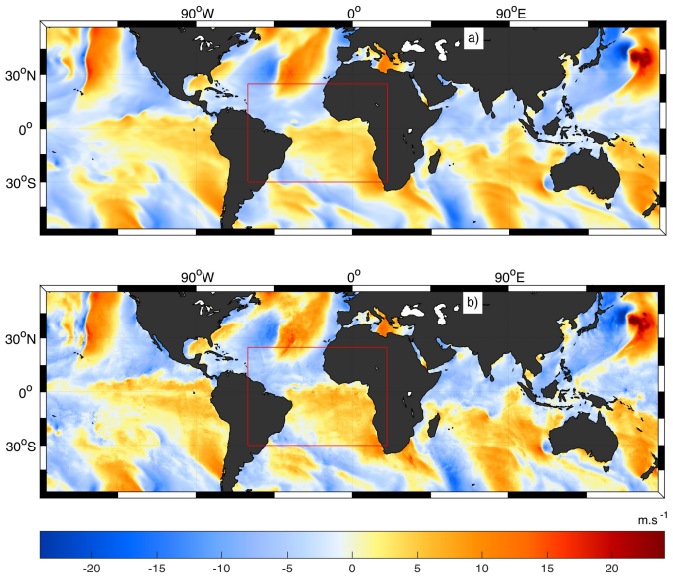

Fig. 2. U10S meridional component for ERAi in 2(a) and ERA* in 2(b) on the 15^{th} January 2013 at 06 UTC. The ERA* map is based on ASCAT-A, ASCAT-B, and OSCAT corrections over a one-day temporal window. The red box indicates the area shown in Fig. 3.

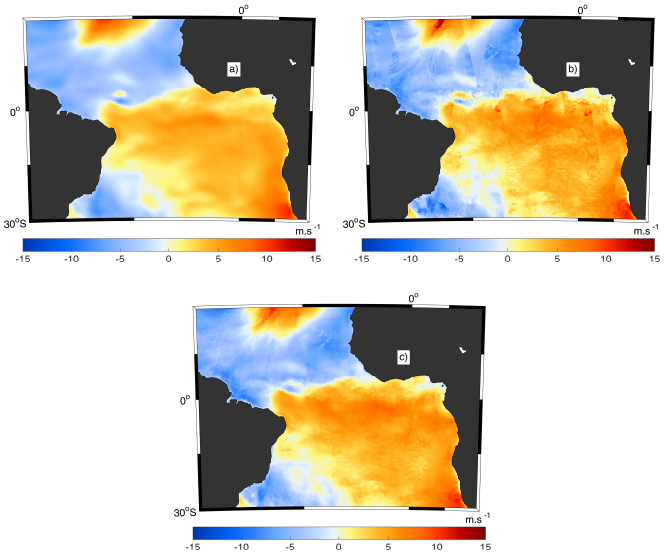

Fig. 3. U10S meridional component over the West African coast for the ERAi in 3(a) and ERA* in 3(b) products shown in Fig. 2 (see red box). The ERA* shown in 3(c) is the same as that of 3(b) but for a SC over a three-day temporal window (N3). The winds are truncated beyond [-15 15] $m.s^{-1}$ to better highlight the differences between the three maps.

OSCAT at 12:00 am/12:00 pm. The use of ASCAT-A/B and OSCAT together substantially increases the local sampling, but is insufficient to fully capture the diurnal cycle as these sensors sample the same location of the ocean with only a 2:30 hours difference. However, if the model diurnal cycle is reasonable and local biases are persistent over longer periods (6-12 hours), then the scatterometer-based corrections would lead to a reduction of model errors at HSCAT verification times, which are 3:30 and 6:00 hours apart from ASCAT-A/B and OSCAT, respectively. Furthermore, if these local biases are persistent over several days, then the ERA* product generated with a larger temporal window (of several days) would be of higher quality than that generated with a one-day temporal window, since the former has a better downsampling of the mesoscale weather variability than the latter.

Figure 4 shows the vector root-mean-square difference (VRMS) between the different ERA* configurations (see legend) and HSCAT U10S as a function of the temporal window size (in days), for the tropics (left), the middle latitudes (middle) and both the tropics and the middle latitudes (right). Figs 4(a), 4(b) and 4(c) (Fig. 4(b), 4(e) and 4(f)) correspond to collocations with HSCAT ascending (descending) passes, thus collocations at 6pm (6am) local time. For reference, the VRMS between ERA and HSCAT is plotted with a thick black solid horizontal line. The latter is used as benchmark, i.e., only those ERA* configurations below the black line are of higher quality (with respect to HSCAT) than ERAi.

For a single-SC, ERA* (orange curves) is very much dependent on the temporal window size, indicating that the weather downsampling of a single scatterometer over one day is rather poor and therefore a larger temporal window is required to reduce the model weather errors. Note the abrupt drop in VRMS that occurs if the ERA* is generated with a correction based on up to three days of accumulated scatterometer information. In particular, a 4-5 day window (N4 or N5) is needed to outperform ERAi. Interestingly, although the scatterometer sampling is larger in the middle latitudes than in the tropics, the ERA* quality for N1 and N2 is more degraded in the former. This is because of the transient weather in the middle latitudes (see e.g., [9]). As a result, a larger number of observations per grid point is required here to reduce model weather errors. When only one scatterometer is available, enhanced sampling is achieved by using larger temporal windows. Note that for a single ASCAT scatterometer or for its predecessor ERS scatterometer, with about half the coverage, longer than 5-day sampling period would be profitable to further improve the bias estimates.

As expected, when adding more scatterometers, the model weather errors are considerably reduced at N1. In particular, when complementary scatterometer orbits are used in the corrections, the derived ERA* products (see purple and blue curves in Fig. 4 as well as the bias and standard deviation scores in Table II) outperform ERAi at N1. In this table we decompose the VRMS in the bias and standard deviation of each wind component and present the scores for HSCAT ascending and descending orbits together. In fact, for such ERA* products, the quality of the data does not significantly depend on the temporal window size, except in the tropics where a slightly higher quality U10S is achieved at N2 or N3. This is probably due to a compensation effect: on the one hand, the larger the temporal window, the larger is the sampling; on the other hand, the larger the temporal window, the more sensitive the system is to local bias changes. Specifically, the mid-latitude local biases seem to be less persistent than those in the tropics, since no further ERA* quality improvements are discernible at temporal windows larger than N1. This may be caused by the impact of fast evolving weather not well captured by ERAi, e.g., mislocation of mid-latitude synoptic variability. Note however that the improvements brought by ERA* over ERAi remain substantial and significant over the entire domain.

Most of the features discussed so far imply that this method is regionally dependent, i.e., its effectiveness is mainly modulated by weather sampling and on the longer term by local bias persistence. Since the biases persist quite well over time, large sampling is essential to improve these bias estimates both in the tropics and in the middle latitudes. Overall this is reflected by the VRMS between the ERA* configurations and HSCAT when compared with the VRMS between ERAi and HSCAT, displayed in Fig. 4.

C. U10S spectra

The verification against independent scatterometer data presented in the previous section shows a significant reduction of model errors, in particular when complementary scatterometer data are used to correct the U10S in the tropics. These findings support that overall most of the high frequency signal observed in the qualitative assessment of the derived ERA* maps (discussed in section IV-A) is dominated by true ocean-related wind signal rather than by noise.

In this section, the derived ERA* U10S fields are assessed in terms of their geophysical consistency and effective resolution, using spectral analysis. Note that only the results for the zonal U10S component are shown, but the same conclusions can be drawn for the meridional component.

In line with [7], to obtain the U10S spectra, valid samples of the U10S components are collected over a month (January 2013) in the HSCAT along-track direction for each across-track wind vector cell (WVC). To comply with the assumption of periodicity imposed when using FFT, a linear transformation detrending method is applied to the samples. Figure 5 shows the final spectra, i.e., the individual spectra averaged over all WVC numbers across the swath and over the mentioned time period. Overall, for HSCAT, 1374 (7455) individual spectra were averaged in the tropics (extra-tropics). Likewise, for ASCAT we average 23812 (72807) individual spectra. The substantially larger number of individual spectra used for ASCAT with respect to HSCAT is due to the much lower QC rejection rate (see section II). Note that the SC field contains both ascending and descending passes and hence many swath edges implied in ERA* cross the HSCAT samples, potentially causing a white noise (flat) spectrum tail when insufficiently sampled.

In particular, this Figure shows the spectra for the zonal U10S component (u) in the tropics (Fig. 5(a)) and the mid-latitudes (Fig. 5(b)) for a fixed combination of scatterometers

(i.e., ASCAT-A, ASCAT-B, and OSCAT) and for various temporal window sizes (see the last row of Table I).

The solid lines show the model U10S spectra for the same sample length (128) as those collected for the HSCAT data (dashed blue), while for the ASCAT-B 12.5 km (dashed purple) a sample size of length 256 is used. The red solid line shows the ERAi spectrum, while the different ERA* configurations (sorted as in the last row of Table I) are shown in green, magenta, orange, cyan and brown. The black dashed line shows the spectral slope of $k^{-5/3}$ for comparison. Note that wave number spectra need periodicity and sufficient samples, which implies artificial numerical closure ([40]). As such, data detrending and sampling can lead to vertical offsets in the spectra. In Fig. 5, the noticeable vertical offset between ASCAT and the other spectral curves is mainly due to sampling. That is, while HSCAT winds are collocated with both ERAi and ERA* winds, ASCAT winds are not (i.e., ASCAT and HSCAT orbits are rather complementary). Note that the swath width and QC differences between HSCAT and ASCAT lead to very different sampling patterns.

Globally, a spectral slope close to $k^{-5/3}$ is reported by [41] for aircraft wind measurements, and by [7] for the ASCAT coastal U10S product at scales below 500 km, as they follow Kolmogorov 3D turbulent theory of the atmosphere. While a k^{-2} slope is referenced by several authors, among others, [42] and [43], using QuikSCAT winds, i.e., a previously released instrument with a similar design to that of HSCAT.

Random atmospheric 3D turbulence has a life cycle of a few hours and therefore its not likely captured by the SC (longer time windows), and consequently also not by ERA*. However, wind features coupled to the ocean mesoscales will largely remain, as well as systematic ERAi flow errors, e.g., tied to the slower synoptic weather patterns and large-scale circulation errors [2]. As shown by [44], [45] the spectral slopes for oceanic turbulence tracers such as Sea Surface Temperature (SST) and Sea Surface Salinity (SSS) are typically between -1 and -3. However, whilst both present similar spectral slopes atmospheric turbulence is more energetic (i.e., larger variance) than oceanic turbulence. In that sense, assuming the oceanic turbulence is well captured by the SC (i.e., oceanic features which persist over a few days), one expects gentler slopes in ERA* (i.e., more comparable to those of HSCAT or ASCAT winds) than in ERAi. This is in line with the spectral slopes shown in Fig. 5 for ASCAT (dashed purple) and HSCAT (dashed blue). Also, in line with the ECMWF spectra shown in [7], the ERAi spectra present a steep slope at high frequencies, indicating a lack of spatial scales below 150 km in the model U10S.

The spectral slopes observed for the ERA* in Fig. 5 lay between those of ERAi and the scatterometers, in particular close to that of HSCAT, indicating that ERA* is able to resolve smaller scales than ERAi although the U10S fields are somewhat smoother than those of HSCAT and notably ASCAT. Note also that the shorter the temporal window used in ERA*, the closer the ERA* spectral slope is to that of HSCAT, i.e., a finer scale ERA* product is obtained showing more sampled 3D turbulence or weather, which is undesirable as noted above. However, following the verification carried out in section IV-B, we note that all SC substantially reduce the ERA*-HSCAT differences and hence are associated with persistent biases and not with random 3D atmospheric turbulence. Moreover, only a slight indication of a flat spectrum tail is noticeable at N1 (see green curve in Fig. 5b), which relates to the swath edge signatures. Following Fig. 4, we note that part of the N1 SC variance is not justified, and better ERA* verification is obtained after 2 or 3 days. Seemingly, a small part of the fast and random $k^{-5/3}$ 3D turbulence and convection is present as noise.

Furthermore, the smoothness observed in the derived map of Fig. 3(c) with respect to that of Fig. 3(b) is in agreement with their corresponding spectral slopes in Fig. 5 a) (i.e., the steeper orange curve with respect to the green solid curve).

The dependence of the spectral slope on spatial sampling is analysed in Fig. 6. The spectra for the zonal wind component (u) are displayed for a fixed time window with different combinations of scatterometers, as listed in the first column of Table I, alongside HSCATs (dashed blue) and ERAi (solid red) spectra. As the number of scatterometers used in the corrections increases, the corresponding ERA* spectral slope becomes steeper, i.e., the derived U10S fields become smoother. This is expected since the scatterometer aggregation results in a wind averaging procedure and an improved bias estimate. Furthermore, when OSCAT U10S are aggregated to the ASCAT-based corrections, there is a marked decrease of the spectral slope (see change from the pink to the light-blue curve on Fig. 6(b), i.e., the ERA* field becomes significantly smoother. This is due to the fact that the ASCAT-A and -B winds overlap in space and time on the weather scale and since OSCAT winds are of lower resolution than ASCAT winds [7]. In any case, by comparing Figs. 4, 5 and 6, it is clear that both the size of the temporal window and the number of scatterometers used can have a pronounced effect on the spectral slope and quality of the ERA* product.

Note also that whether we fix the number of scatterometers (Fig. 5) or the time window (Fig. 6), the spectra in the middle latitudes are more energetic at small wave numbers than those in the tropics, due to the presence of large-scale systems, still the same conclusions can be drawn in terms of spectral slopes. The exception is found for the ERA*$_A$N1 product spectra, which at mid-latitudes is slightly less steep than that of HSCAT. This is a very energetic region characterized by the presence of fast evolving systems, in which a product configuration using a single scatterometer for a one day mean correction is likely to also be affected by the previously mentioned weather sampling artifacts.

In order to correct for persistent model biases at the oceanic mesoscale, the accumulation time window is strictly dependent on the longevity of such biases. In that sense, from the geophysical perspective, taking into consideration the spectral analysis presented here, the relatively high VRMS values for ERA*$_A$N1 or ERA*$_A$N2 shown in Fig. 4 indicate that the high-frequency variance depicted by spectral analysis is dominated by weather sampling artifacts rather than by ocean-related small-scale wind signal, particularly for the middle latitudes. Additionally, the same statistics suggest that for ERA*$_{ABO}$N1 the significant reduction of the local biases is

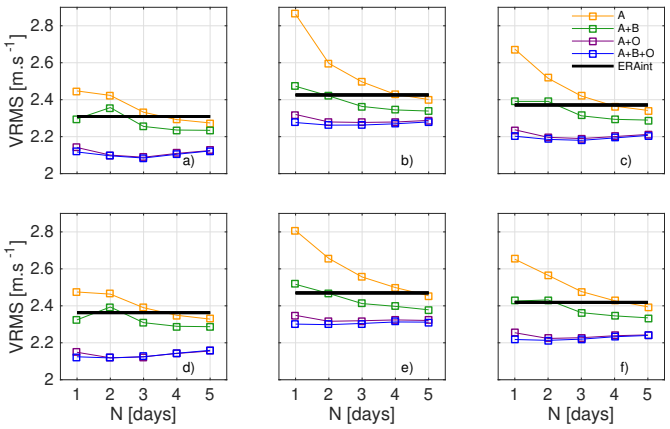

Fig. 4. Estimated Vector root mean square (VRMS in ms^{-1}) difference between different ERAi/ERA* U10S products and HSCAT U10S ascending (top) and descending (bottom) passes as a function of the SC temporal window size, over an eight day period, for the tropics (a and d), the middle latitudes (b and e), and both the tropics and the middle latitudes [-55° to 55°] (c and f). The different colour lines show the VRMS scores for ERA (black line in bold), ERA* configuration using only ASCAT-A (orange line), ERA* using ASCAT-A and B (green line), ERA* using ASCAT-A and OSCAT (purple), and ERA* using ASCAT-A, ASCAT-B and OSCAT (blue).

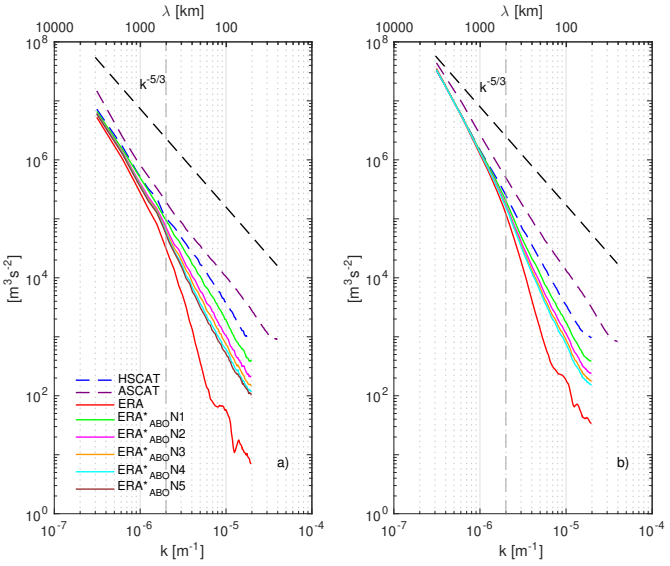

Fig. 5. Power density spectra for the zonal U10S component (u) of HSCAT (dashed blue), ASCAT-B (dashed purple), and collocated ERAi (red) and ERA* (see colour legend) products, in the tropics 5(a) and the middle latitudes 5(b). The ERA* products based on combined ASCAT-A, ASCAT-B and OSCAT (ABO notation) SC for different temporal windows are shown. The ERA*$_{ABO}$N notation from N1 to N5 corresponds respectively to SC temporal windows from 1 to 5 days (see Table I).

at odds with the observed shallow spectral slopes (comparable to those of HSCAT, measuring 3D turbulence due to weather), and where a visual inspection of the derived maps indeed reveals the presence of swath-generated artifacts likely due to relatively poor scatterometer weather averaging. A reasonable trade-off between the spatial/temporal sampling and the accuracy/consistency of the derived maps is the ERA* based on a 2-3 days (N2 or N3) time window for ERA*$_{ABO}$, while longer windows are necessary for fewer scatterometers.

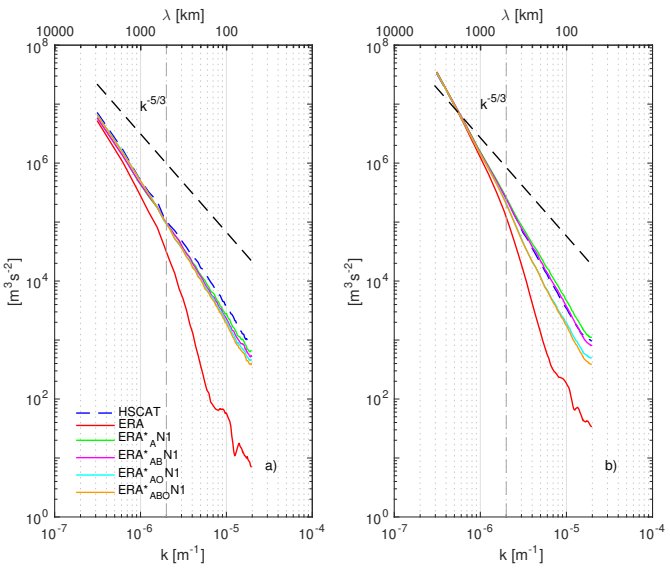

Fig. 6. Power density spectra for the zonal U10S component (u) of HSCAT (dashed blue) and collocated ERAi (red) and ERA* (see colour legend) products, in the tropics 6(a) and the middle latitudes 6(b). The different ERA* configurations shown here use a one-day SC temporal window (see notation in Table I).

V. Conclusion

A new approach, which uses scatterometer data to correct for persistent local NWP wind vector biases, is proposed in this study. The new ERA* product is shown to be of higher resolution and accuracy than the original ERAi product, both in the tropics and the middle latitudes.

The proposed method, which uses geo-located temporally averaged U10S component differences between different scatterometer wind sources and collocated ERAi U10S, is able to introduce true smaller scale signal into ERA*, which corresponds to the physical processes absent or misrepresented by ERAi, e.g., strong current effects (such as WBCS, highly stationary), wind effects associated to the ocean mesoscales (SST), coastal effects (land see breezes, katabatic winds), parameterization errors and large-scale circulation effects, e.g., at the ITCZ.

Several ERA* configurations using different scatterometer combinations and temporal window sizes (over which the scatterometer corrections are performed) are tested. All ERA* configurations are then verified against independent HSCAT U10S data while the geophysical consistency of the U10S maps is assessed by spectral analysis. All ERA* configurations reveal enhanced mesoscale variability with respect to the original ERAi. The versions with multiple scatterometers show a significant reduction of about 10% in the VRMS values (against HSCAT) values when compared to those of ERAi. For single scatterometers, the VRMS keeps reducing after 5 days and longer averaging periods will be beneficial.

Overall, the ERA* generated with a single scatterometer (ASCAT-A) needs a 4-5 day window (N4 to N5) to outperform ERAi, and despite the larger scatterometer sampling in the middle latitudes with respect to the tropics, the ERA* quality degradation with respect to ERAi is more pronounced in the

TABLE II
MEAN (b) AND STANDARD DEVIATION (ϵ) OF THE DIFFERENCES BETWEEN DIFFERENT ERAI/ERA* PRODUCTS AND HSCAT, IN THE TROPICS AND THE MID-LATITUDES FOR BOTH ZONAL (u) AND MERIDIONAL (v) U10S COMPONENTS. THE NUMBERS OF VALID WINDS OVER WHICH THE STATISTICS ARE COMPUTED ARE SHOWN IN BRACKETS.

	mid-lat. (2331603)				tropics (2131292)			
ASC & DSC	$b_u(ms^{-1})$	$\epsilon_u(ms^{-1})$	$b_v(ms^{-1})$	$\epsilon_v(ms^{-1})$	$b_u(ms^{-1})$	$\epsilon_u(ms^{-1})$	$b_v(ms^{-1})$	$\epsilon_v(ms^{-1})$
ERA*$_{ABO}N1$	0.086	1.589	0.014	1.645	0.031	1.471	-0.041	1.527
ERA*$_{ABO}N3$	0.084	1.611	0.012	1.616	0.023	1.450	-0.051	1.513
ERA	0.546	1.703	0.161	1.663	-0.035	1.596	-0.032	1.705

former for N1 and N2. This is likely due to the transient character of weather phenomena at these latitudes, i.e., [2] point that ERA products show deficient zonal and meridional wind variabilities, over the storm tracks, where wind variations generate westward baroclinic Rossby flow, which confine upper ocean response establishing the WBCS.

As to the geophysical consistency of the ERA*, the observed spectral slopes consistently lay between those of the scatterometers and ERAi, although closer to the former, indicating that the ERA* gridded fields maintain the spatial scales resolved by scatterometers. However, only the persistent small scales are kept in the SC, which are due to oceanic features such as wind changes over SST gradients and ocean currents. A persistence correction cannot bring lacking 3D atmospheric turbulence and moist convection as these processes are fast. These effects are however visible in the standard deviation of the SC and may be used to represent ocean forcing due to atmospheric variability [46], which is substantial and here left to future work.

As shown in the qualitative analysis and then verified in the spectral analysis, the use of larger temporal windows generates significantly smoother U10S fields through increased sampling and leads to similar quality when verified against HSCAT. This is particularly noticeable for the tropics. A temporal window larger than N1 is necessary to avoid the reported swath-generated artifacts and average out the fast and transient weather effects.

The U10S spectra also show a slight smoothening effect on the ERA* U10S fields when increasing the number of scatterometers used in the corrections. However, this effect, which does not significantly depend on the temporal window size, is very small, both in tropics and the middle latitudes. Moreover, the multiple scatterometer configurations show a clear benefit in terms of VRMS scores, indicating that these are the most suitable configurations (when available), where mixing Ku- and C-band scatterometers appears no limitation.

Based on the results from the statistical and spectral analyses, a suitable configuration may use complementary scatterometers and a temporal window of two or three days. In particular, ERA*$_{ABO}$N2 or N3 show a good compromise between resolved spatial scales and data quality (best agreement with respect to independent verification), i.e., with our spectral slopes close those of the HSCAT, smaller scales are present in the new product because the signature of oceanic mesoscale features is imprinted in the atmosphere, as was previously shown by [14] with SeaWinds. Longer time windows will slowly blur the ocean-related processes captured in the scatterometer winds.

This method shows potential, particularly in regions of persistent local conditions, e.g., tropics and the trade winds region. For operational purposes, and with the current increase of scatterometer sampling (in 2019, seven scatterometers are expected to operate in orbit), evidence suggests that improvement can be achieved by increasing the number of scatterometers, while reducing the temporal window of the correction. For the middle latitudes, further research will focus on characterizing the impact of, on the one hand, increased sampling and, on the other, the presence of transient weather phenomena, on the ERA* quality. This can be done through simulations. Furthermore, alternative scatterometer corrections based on process attribution, e.g., accounting for atmospheric stability parameterization errors, will be tested in order to improve the quality of ERA*.

Another planned activity is to use the recently available ERA5 data set, i.e., the new ECMWF reanalysis which includes the latest model and data assimilation scheme updates, instead of ERAi to produce ERA* U10S. Although recent analysis shows that the reported local biases in ERAi are still present in ERA5, they are smaller in amplitude ([2]), which indicates that a different ERA* configuration (in terms of scatterometer sampling and temporal window size) may be more optimal. This needs further investigation.

Moreover, the ERA* forcing product should be tested in a regional ocean model simulation, particularly the ERA*$_{ABO}$N2 and ERA*$_{ABO}$N3 configurations, to show the added value of ERA* with respect to currently used NWP-based forcing.

Finally, a modified SC may be implemented as a variational geographically-based vector wind bias correction during NWP data assimilation. Note in particular, that the here reported 10% reduction in observation minus background RMS differences would represent substantial progress in NWP scatterometer data assimilation

ACKNOWLEDGMENT

The work was supported by the Spanish Research and Development Plan under the FPI grant (BES-2013-064521) from the project MIDAS-7 (reference AYA2012-39356-C05-03) and the R&D project L-BAND (reference ESP2017-89463-C3-2-R). The authors would like to thank the Chinese National Satellite Ocean Application Service (NSOAS) for providing the HY-2A L1B data. They would also like to

acknowledge Dr. Jos de Kloe (KNMI) for his support with the wind processors from the Eumetsat Numerical Weather Prediction Satellite Application Facility (NWP-SAF), i.e., the ASCAT Wind Data Processor (AWDP) and the Pencil-beam Wind Processor (PenWP).

REFERENCES

[1] L. H. Kantha and C. A. Clayson, Eds., *Numerical models of oceans and oceanic processes*. Elsevier, 2000, vol. 66, ch. 2, pp. 127–245.

[2] M. Belmonte Rivas and A. Stoffelen, "Characterizing ERA-interim and ERA5 surface wind biases using ASCAT," *Ocean Science*, vol. 15, no. 3, pp. 831–852, 2019.

[3] G. P. King, M. Portabella, W. Lin, and A. Stoffelen, "Correlating extremes in wind and stress divergence with extremes in rain over the Tropical Atlantic," pp. 1–35.

[4] H. Hersbach, "Comparison of C-Band scatterometer CMOD5.N equivalent neutral winds with ECMWF," *Journal of Atmospheric and Oceanic Technology*, vol. 27, no. 4, pp. 721–736, 2010.

[5] A. R. Brown, A. C. M. Beljaars, H. Hersbach, H. A., M. Miller, and D. Vasiljevic, "Wind turning across the marine atmospheric boundary layer," *Q.J.R. Meteorol. Soc.*, vol. 131, no. 607, pp. 1233–1250, 2005.

[6] I. Sandu, A. Beljaars, P. Bechtold, T. Mauritsen, and G. Balsamo, "Why is it so difficult to represent stably stratified conditions in numerical weather prediction (NWP) models?" *Journal of Advances in Modeling Earth Systems*, vol. 5, no. 2, pp. 117–133, 2013.

[7] J. Vogelzang, A. Stoffelen, A. Verhoef, and J. Figa-Saldaña, "On the quality of high-resolution scatterometer winds," *Journal of Geophysical Research: Oceans*, vol. 116, no. C10033, 2011.

[8] W. Lin, M. Portabella, A. Stoffelen, A. Verhoef, and A. Turiel, "ASCAT wind quality control near rain," *IEEE Trans. Geosci. Remote Sens.*, vol. 53, no. 8, pp. 4165–4177, Aug 2015.

[9] M. Portabella and A. Stoffelen, "On scatterometer Ocean Stress," *Journal of Atmospheric and Ocean Technology*, vol. 26, no. 2, pp. 368–382, February 2009.

[10] K. A. Kelly, S. Dickinson, M. J. McPhaden, and G. C. Johnson, "Ocean currents evident in satellite wind data," *Geophysical Research Letters*, vol. 28, no. 12, pp. 2469–2472, 2001.

[11] D. B. Chelton and M. H. Freilich, "Scatterometer-based assessment of 10-m wind analyses from the operational ECMWF and NCEP numerical weather prediction models," *Monthly Weather Review*, vol. 133, no. 2, pp. 409–429, 2005.

[12] D. B. Chelton and S.-P. Xie, "Coupled ocean-atmosphere interaction at oceanic mesoscales," *Oceanography*, vol. 23, no. 4, pp. 52–69, December 2010.

[13] J. Vogelzang, G. P. King, and A. Stoffelen, "Spatial variances of wind fields and their relation to second-order structure functions and spectra," *Journal of Geophysical Research: Oceans*, vol. 120, no. 2, pp. 1048–1064, 2015.

[14] D. B. Chelton, M. G. Schlax, M. H. Freilich, and R. F. Milliff, "Satellite measurements reveal persistent small-scale features in ocean winds," *Science*, vol. 303, no. 5660, pp. 978–983, 2004.

[15] A. Stoffelen and J. Vogelzang, "Wind bias correction guide," EUMETSAT-NWP SAF report v1.3, NWPSAF-KN-UD-007, Set 2018.

[16] V. J. Stoffelen, A. and G.-J. Marseille, "High resolution data assimilation guide," EUMETSAT-NWP SAF report v1.2, NWPSAF-KN-UD-008, Set 2018.

[17] J. Figa-Saldaña, J. Wilson, E. Attema, R. Gelsthorpe, M. Drinkwater, and A. Stoffelen, "The advanced scatterometer (ASCAT) on the meteorological operational (MetOP) platform: A follow on for european wind scatterometers," Technical Note: Can. J. Remote Sensing, pp. 404–412, 2002.

[18] D. P. Dee, S. M. Uppala, A. J. Simmons, P. Berrisford, P. Poli, S. Kobayashi, U. Andrae, M. A. Balmaseda, G. Balsamo, P. Bauer, P. Bechtold, A. C. M. Beljaars, L. van de Berg, J. Bidlot, N. Bormann, C. Delsol, R. Dragani, M. Fuentes, A. J. Geer, L. Haimberger, S. B. Healy, H. Hersbach, E. V. Hlm, L. Isaksen, P. Kllberg, M. Khler, M. Matricardi, A. P. McNally, B. M. Monge-Sanz, J.-J. Morcrette, B.-K. Park, C. Peubey, P. de Rosnay, C. Tavolato, J.-N. Thpaut, and F. Vitart, "The ERA-Interim reanalysis: configuration and performance of the data assimilation system," *Quarterly Journal of the Royal Meteorological Society*, vol. 137, no. 656, pp. 553–597, 2011.

[19] J. De Kloe, A. Stoffelen, and A. Verhoef, "Improved use of scatterometer measurements by using stress-equivalent reference winds," *IEEE Journal of Selected Topics in Applied Earth Obs and Remote Sensing*, vol. 10, no. 5, pp. 2340–2347, May 2017.

[20] W. Tang, W. T. Liu, B. Stiles, and A. Fore, "Detection of diurnal cycle of ocean surface wind from space-based observations," *International Journal of Remote Sensing*, vol. 35, no. 14, pp. 5328–5341, 2014.

[21] S. Gille, S. Nguyen, D. Northcott, J. Nutt, and A. Subramanian, "Diurnal wind variability from RapidScat," in *International Ocean Vector Winds Science Team Meeting*, 2016.

[22] M. Portabella, A. Stoffelen, W. Lin, A. Turiel, J. V. A. Verhoef, and J. Ballabrera, "Rain effects on ASCAT-retrieved winds: toward an improved quality control," *IEEE Transactions on Geoscience and Remote Sensing*, vol. 50, no. 7, pp. 2495–2506, 2012.

[23] J. E. Stopa, A. A. Mouche, B. Chapron, and F. Collard, "Sea state impacts on wind speed retrievals from C-Band radars," *IEEE Journal of Selected Topics in Applied Earth Observations and Remote Sensing*, vol. 10, no. 5, pp. 2147–2155, May 2017.

[24] M. Portabella and A. Stoffelen, "Rain detection and quality control of SeaWinds," *Journal of Atmospheric and Oceanic Technology*, vol. 18, no. 7, pp. 1171–1183, 2001.

[25] B. W. Stiles and R. S. Dunbar, "A neuranl network technique for improving the accuracy of scatterometer winds in rainy conditions," *IEEE Transactions on Geoscience and Remote Sensing*, vol. 48, no. 8, pp. 3114–3122, Aug 2010.

[26] W. Lin and M. Portabella, "Toward an improved wind quality control for RapidScat," *IEEE Transactions on Geoscience and Remote Sensing*, vol. 55, no. 7, pp. 3922–3930, July 2017.

[27] Z. Wang, A. Stoffelen, C. Zhao, J. Vogelzang, A. Verhoef, J. Verspeek, M. Lin, and G. Chen, "An SST-dependent Ku-band geophysical model function for RapidScat," *Journal of Geophysical Research: Oceans*, vol. 122, no. 4, pp. 3461–3480, 2017.

[28] Z. Wang, A. Stoffelen, F. Fois, A. Verhoef, C. Zhao, M. Lin, and G. Chen, "SST dependence of Ku- and C-band backscatter measurements," *IEEE Journal of Selected Topics in Applied Earth Observations and Remote Sensing*, vol. 10, no. 5, pp. 2135–2146, May 2017.

[29] M. Portabella, A. Stoffelen, A. Verhoef, and J. Verspeek, "A new method for improving scatterometer wind quality control," *IEEE Geoscience and Remote Sensing Letters*, vol. 9, pp. 579–583, 07 2012.

[30] A. Verhoef, J. Vogelzang, and A. Stoffelen, "Oceansat-2 L2 winds Data Record validation report," EUMETSAT- OSI SAF, report, June 2017.

[31] M. Portabella and A. Stoffelen, "A probabilistic approach for SeaWinds data assimilation," *Quarterly Journal of the Royal Meteorological Society*, vol. 130, pp. 127–152, 01 2004.

[32] A. Verhoef, M. Portabella, and A. Stofellen, "High-resolution ASCAT scatterometer winds near the coast," *IEEE Trans. Geosci. Remote Sens.*, vol. 50, no. 7, pp. 2481–2487, Jul 2012.

[33] J. Zhu, X. Dong, and R. Yun, "Calibration and validation of the HY-2 scatterometer backscatter measurements over ocean," in *proc. IEEE Geoscience and Remote Sensing Symposium*, July 2014, pp. 4382–4385.

[34] W. Lin, M. Portabella, A. Stoffelen, A. Verhoef, S. Lang, Y. Zhang, and M. Lin, "On the improvement of the HY-2A scatterometer wind quality control," in *proc. IEEE International Geoscience and Remote Sensing Symposium (IGARSS)*, July 2016, pp. 407–410.

[35] H. Wang, Z. Jianhua, M. Lin, H. Xiaoqi, Y. Zhao, C. Chuntao, Y. Zhang, and H. Peng, "First six months quality assessment of HY-2A SCAT wind products using in situ measurements," *Acta Oceanologica Sinica*, vol. 32, pp. 27–33, 11 2013.

[36] A. C. Beljaars, "Air-sea interaction in the ECMWF model," in *Proc. Seminar on Atmosphere–Surface Interaction, ECMWF*, 1997, pp. 33–52.

[37] F. D. Biasio, M. Bajo, S. Vignudelli, G. Umgiesser, and S. Zecchetto, "Improvements of storm surge forecasting in the Gulf of Venice exploiting the potential of satellite data: the ESA DUE eSurge-Venice project," *European Journal of Remote Sensing*, vol. 50, no. 1, pp. 428–441, 2017.

[38] M. Bajo, F. D. Biasio, G. Umgiesser, S. Vignudelli, and S. Zecchetto, "Impact of using scatterometer and altimeter data on storm surge forecasting," *Ocean Modelling*, vol. 113, pp. 85–94, 2017.

[39] W. Lin, M. Portabella, A. Stoffelen, A. Vogelzang, and A. Verhoef, "ASCAT wind quality under high subcell wind variability conditions," *Journal of Geophysical Reseach: Oceans*, vol. 120, pp. 1–16, 2015.

[40] J. Volgenzang, "How to calculate wind spectra," EUMETSAT-NWP SAF report v1.1, NWPSAF-KN-TR-008, April 2013.

[41] G. Nastrom and K. S. Gage, "A climatology of atmospheric wave number spectra of wind and temperature observed by commercial aircraft," *J. Atmos. Sci*, vol. 42, pp. 950–960, 1985.

[42] J. Patoux and R. A. Brown, "Spectral analysis of QuikSCAT surface winds and two-dimensional turbulence," *J. Geophys. Res.*, vol. 106, no. D20, pp. 23 995–24 005, 2001.

[43] D. B. Chelton, M. H. Freilich, J. M. Sienkiewicz, and J. M. Von Ahn, "On the Use of QuikSCAT Scatterometer Measurements of Surface Winds for Marine Weather Prediction," *Monthly Weather Review*, vol. 134, no. 8, pp. 2055–2071, 2006.
[44] R. W. Reynolds and D. B. Chelton, "Comparisons of daily sea surface temperature analyses for 2007-08," *Journal of Climate*, vol. 23, no. 13, pp. 3545–3562, 2010.
[45] N. Hoareau, A. Turiel, M. Portabella, J. Ballabrera-Poy, and J. Vogelzang, "Singularity power spectra: a method to assess geophysical consistency of gridded productsapplication to sea-surface salinity remote sensing maps," *IEEE Trans. Geosci. Rem. Sens.*, vol. 56, no. 9, pp. 5525–5536, Sep 2018.
[46] R. F. Milliff, J. Morzel, D. B. Chelton, and M. H. Freilich, "Wind stress curl and divergence biases from rain effects on QuikSCAT surface wind retrievals," *J. Atmos. Oceanic Technol.*, vol. 21, pp. 1216–1231, 2004.

Ana Trindade was born in Portugal in 1985. She received a B.Sc. degree in Meteorology, Oceanography and Geophysics from the University of Lisbon, Lisbon, Portugal, in 2008, the M.Sc. degree in Geophysical Sciences from the University of Lisbon, Lisbon, Portugal, in 2011. She is currently a Ph.D student in physics at the University of Barcelona, Barcelona, Spain, working on scatterometery and ocean forcing products.

Marcos Portabella was born in Spain in 1970. He received the B.Sc. degree in physics from the University of Barcelona, Barcelona, Spain, in 1994, the M.Sc. degree in remote sensing from the Institute of Space Studies of Catalonia, Barcelona, in 1995, and the Ph.D. degree in physics from the University of Barcelona. He is currently with the Institut de Ciències del Mar, Barcelona, involved in satellite remote sensing, and particularly in scatterometry and L-band radiometry.

Ad Stoffelen was born on February 25, 1962 in The Netherlands. He received the M.Sc. degree in physics from the Technical University of Eindhoven, Eindhoven, The Netherlands, in 1987 and the Ph.D. degree in meteorology on scatterometry from the University of Utrecht, Utrecht, The Netherlands. He is currently working with Royal Netherlands Meteorological Institute and responsible for the ASCAT wind products. His research interests include European Space Agency ADM-Aeolus Doppler Wind Lidar mission.

Wenming Lin was born on April 22, 1984, in China. He received the B.Sc. degree in engineering from Wuhan University, Wuhan, China, in 2006 and the Ph.D. degree in engineering from the National Space Science Center, Chinese Academy of Sciences, Beijing, China, in 2011.,He was a Postdoctoral Researcher with the Institute of Marine Sciences, Barcelona, Spain, and now working at NUIST, Nanjing, China, on the advanced oceanographic data processing methods, remote sensing of ocean surface winds, and data assimilation.

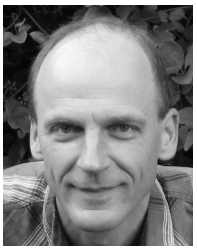

Anton Verhoef was born on Dec 10, 1964, in The Netherlands. He received the M.Sc. degree in physics from Rijksuniversiteit Groningen, Groningen, The Netherlands, in 1989 and the Ph.D. degree in solid state physics from Rijksuniversiteit Groiningen in 1994. He is currently with Royal Netherlands Meteorological Institute and working on scatterometry processing software development, data validation, quality monitoring, and user services.